



RESEARCH PAPER

The role of Rubisco kinetics and pyrenoid morphology in shaping the CCM of haptophyte microalgae

Ana M.C. Heureux^{1,*†}, Jodi N. Young², Spencer M. Whitney³, Maeve R. Eason-Hubbard¹,
Renee B.Y. Lee^{1,4}, Robert E. Sharwood³ and Rosalind E.M. Rickaby¹

¹ University of Oxford, Department of Earth Sciences, South Parks Road, Oxford OX1 3AN, UK

² University of Washington, School of Oceanography, Seattle, WA 98195, USA

³ ARC Centre of Excellence for Translational Photosynthesis, Research School of Biology, Australian National University, Canberra ACT 2601, Australia

⁴ University of Reading, School of Biological Sciences, Reading, Berkshire RG6 6U, UK

[†] Present address: University of Hawai'i at Hilo, College of Agriculture, Forestry and Natural Resource Management, 200 W. Kawili St, Hilo, HI 96720, USA.

* Correspondence: aheureux@gmail.com

Received 25 January 2017; Editorial decision 2 May 2017; Accepted 15 May 2017

Editor: Howard Griffiths, University of Cambridge

Abstract

The haptophyte algae are a cosmopolitan group of primary producers that contribute significantly to the marine carbon cycle and play a major role in paleo-climate studies. Despite their global importance, little is known about carbon assimilation in haptophytes, in particular the kinetics of their Form 1D CO₂-fixing enzyme, Rubisco. Here we examine Rubisco properties of three haptophytes with a range of pyrenoid morphologies (*Pleurochrysis carterae*, *Tisochrysis lutea*, and *Pavlova lutheri*) and the diatom *Phaeodactylum tricornutum* that exhibit contrasting sensitivities to the trade-offs between substrate affinity (K_m) and turnover rate (k_{cat}) for both CO₂ and O₂. The pyrenoid-containing *T. lutea* and *P. carterae* showed lower Rubisco content and carboxylation properties (K_C and k_{cat}^C) comparable with those of Form 1D-containing non-green algae. In contrast, the pyrenoid-lacking *P. lutheri* produced Rubisco in 3-fold higher amounts, and displayed a Form 1B Rubisco k_{cat}^C – K_C relationship and increased CO₂/O₂ specificity that, when modeled in the context of a C₃ leaf, supported equivalent rates of photosynthesis to higher plant Rubisco. Correlation between the differing Rubisco properties and the occurrence and localization of pyrenoids with differing intracellular CO₂:O₂ microenvironments has probably influenced the divergent evolution of Form 1B and 1D Rubisco kinetics.

Key words: Algae, carbon-concentrating mechanisms, Haptophyta, pyrenoid, Rubisco.

Introduction

The CO₂-fixing enzyme Rubisco (EC 4.1.1.39) evolved in the Archaean Eon when the atmosphere lacked O₂, and CO₂ was estimated to be 50-fold higher than current levels (Berner and Canfield, 1989; Berner, 2006; Tabita *et al.*, 2008). With the evolution of O₂-producing photosynthesis around the early Proterozoic

(2.5 Gya), atmospheric O₂ increased while the CO₂ concentration declined (Canfield, 2005) (Fig. 1). The diminishing atmospheric CO₂:O₂ ratio negatively influenced Rubisco catalysis, as its photosynthetic CO₂-fixing function is competitively inhibited by O₂ to produce 2-phosphoglycolate (2-PG) (Tcherkez *et al.*,

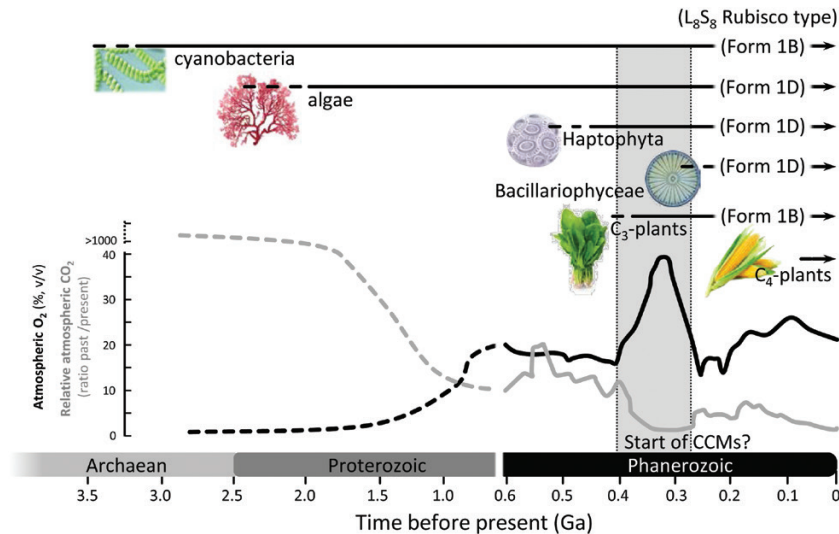


Fig. 1. Rubisco evolution and catalysis. Geological history of the past versus present atmospheric [CO₂] (gray) and percentage atmospheric O₂ (% v/v) (black; modified from [Berner and Canfield, 1989](#); [Badger et al., 2002](#); [Whitney et al., 2011](#)) highlighting the estimated appearance of key primary producers (horizontal lines) ([Yoon et al., 2002, 2004](#); [Liu et al., 2010](#)) their differing Form 1B or 1D Rubisco lineages they produce, and the predicted timing when algal carbon-concentrating mechanisms (CCMs; gray shading) evolved ([Badger et al., 2002](#); [Moritz and Griffiths, 2013](#)).

2006; [Whitney et al., 2011](#); [Sharwood, 2017](#)). Recycling of 2-PG to 3-phosphoglycerate (3-PGA) by photorespiration consumes energy and loses fixed CO₂. A further limitation to Rubisco function in the modern atmosphere is a low affinity for CO₂ and a slow catalytic rate that necessitates high Rubisco concentrations to support adequate rates of photosynthesis ([Reinfelder, 2011](#); [Whitney et al., 2011](#); [Long et al., 2015](#); [Sharwood et al., 2016b](#)).

The catalytic limitations of Rubisco are exacerbated in aquatic ecosystems due to restraints on aqueous CO₂ availability because of slow rates of gas diffusion in water (~10 000 times slower than in air) and reliance on mixing of the water column ([Badger et al., 1998](#)). In addition, increased partitioning of inorganic carbon to HCO₃⁻ with higher pH in aquatic systems diminishes aqueous CO₂ availability. There is evidence of catalytic adaptation by Rubisco in algae to the changing atmospheric CO₂ (and O₂) conditions over geological time scales ([Young et al., 2012](#)). Recent work, however, showed that the characteristic faster CO₂ fixation rates ($k_{\text{cat}}^{\text{C}}$) and lower CO₂ affinities (i.e. higher K_{m} for CO₂; K_{C}) observed in Form 1A and Form 1B Rubisco [e.g. in *Chlamydomonas* with a pyrenoid-based CO₂-concentrating mechanism (CCM)] ([Badger et al., 1998](#); [Ghannoum et al., 2005](#); [Sharwood et al., 2016a](#)) are not shared by diatom Form 1D Rubisco ([Hanson, 2016](#); [Young et al., 2016](#); see also [Fig. 3A](#)). This has led to calls for a more expansive analysis of Rubisco's natural kinetic diversity so that we can fully understand the correlative interactions between specificity for CO₂ as opposed to O₂ ($S_{\text{C/O}}$), $k_{\text{cat}}^{\text{C}}$, and K_{C} . The one-dimensional, linear correlations previously proposed ([Tcherkez et al., 2006](#); [Savir et al., 2010](#)) may actually vary with photosynthetic taxa ([Tcherkez, 2013, 2016](#); [Hanson, 2016](#); [Sharwood, 2017](#)).

In photosynthetic organisms, the CCM arose multiple times in response to a declining atmospheric CO₂:O₂ ratio as a means to increase the CO₂/O₂ environment around Rubisco ([Fig. 1](#)). Data on the anatomical, biochemical, and genomic detail for CCMs in vascular plants with C₄ and Crassulacean

acid metabolism (CAM) physiologies are highly detailed ([von Caemmerer and Furbank, 2016](#)). The high CO₂ environment reduces Rubisco oxygenation and the associated energy costs of photorespiration, allowing the plant to work with lower stomatal conductance and reduced amounts of Rubisco ([Sage et al., 2012](#)). These features allow more efficient use of water, nitrogen, and light, and permit these plants to survive in more arid and nutrient-limited environments ([Sage, 2002](#); [Ghannoum et al., 2005](#); [Lara and Andreo, 2011](#); [Long et al., 2015](#)). The CCM in plants also allowed Form 1B Rubisco to evolve a higher $k_{\text{cat}}^{\text{C}}$ at the expense of a higher K_{C} (i.e. lower CO₂ affinity) with little or no effect on $S_{\text{C/O}}$ ([Sharwood et al., 2016a, b](#)). Curiously this $k_{\text{cat}}^{\text{C}}$ - K_{C} trade-off is not shared by Form 1D Rubisco from diatoms where relatively higher K_{C} values have been retained as a consequence of other environmental pressures (low nutrient and extracellular CO₂ availability) that pose limitations to resource investment into Rubisco ([Young et al., 2016](#)). It is likely that resources other than CO₂, such as nitrogen and light availability, have a strong influence on CCM evolution and regulation ([Raven et al., 2008, 2012](#)).

Understanding how microalgal Rubisco catalysis has differentially evolved remains limited by our understanding of the structural components and effectiveness of the CCM in microalgae. The last few years have seen significant advances in our understanding of CCM in the model freshwater green alga, *Chlamydomonas reinhardtii* ([Engel et al., 2015](#); [Wang et al., 2015](#); [Yamano et al., 2015](#); [Mackinder et al., 2016](#); [Mangan et al., 2016](#); [Wang et al., 2016](#)). To what extent this knowledge is translatable to the CCM of the structurally differing and evolutionarily distinct marine microalgae (e.g. diatoms and haptophytes) remains unclear ([Bedoshvili et al., 2009](#); [Hopkinson et al., 2011, 2013](#)). Currently a completed nuclear haptophyte genome is available for the Isochrysidale *Emiliania huxleyi* ([Read et al., 2013](#)) and a draft genome for the Prymnesiales *Chrysochromulina tobin* ([Hovde et al., 2015](#)). Although less understood, the CCMs of marine microalgae are

known typically to employ a pyrenoid, Rubisco activase, carbonic anhydrase (CA), and inorganic carbon (C_i) transporters to elevate CO_2 levels around Rubisco (Hopkinson *et al.*, 2011; Reinfelder, 2011; Loganathan *et al.*, 2016). The pyrenoid is a proteinaceous body that appears electron dense when examined by TEM and contains most, sometimes all, of the cellular Rubisco (Engel *et al.*, 2015; Mackinder *et al.*, 2016).

In *C. reinhardtii*, HCO_3^- transport occurs via thylakoids and C_i transporters that work in association with pyrenoid CAs to elevate CO_2 around Rubisco (Karlsson *et al.*, 1998; Trimborn *et al.*, 2007; Lee *et al.*, 2013; Wang *et al.*, 2015; Yamano *et al.*, 2015). Physiological and genetic evidence in model diatoms imply that HCO_3^- is pumped into the chloroplast stroma and diffuses into the pyrenoid where it is converted to CO_2 by CA to elevate the $[CO_2]$ around Rubisco (Hopkinson *et al.*, 2011, 2016). Recent identification of a thylakoid lumen-localized CA in *P. tricornutum* further suggests that the pyrenoid-penetrating thylakoids probably provide an important CO_2 supply within the pyrenoids (Kikutani *et al.*, 2016).

What remains unclear is how the pyrenoid structure influences CCM efficiency. In *C. reinhardtii*, the pyrenoid contains a starch sheath (Moroney *et al.*, 2011; Engel *et al.*, 2015) while in diatoms it can comprise a lipid membrane (Bedoshvili

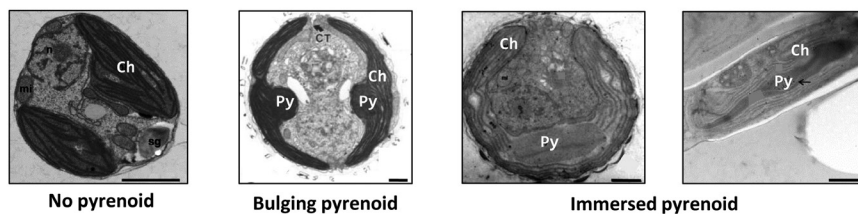
et al., 2009), lack a delimiting structure (Bendif *et al.*, 2011), vary in number and shape, and differ in the presence/structure of traversing thylakoids (Badger *et al.*, 1998). To better understand the relationships between Rubisco kinetics, content, and pyrenoid biology in marine microalgae, we have expanded on our previous study of diatom Rubisco (Young *et al.*, 2016) to include three marine haptophytes that contain bulging (Pleurochrysis carterae), immersed [Tisochrysis lutea, formerly Isocrysis sp. strain CS-177 (Bendif *et al.*, 2013)], or no pyrenoid (Pavlova lutheri) within their chloroplast and varying numbers and location of pyrenoid-traversing thylakoids (Fig. 2A).

Materials and methods

Algae culturing

Cultures of the haptophytes *P. lutheri* (CS-182), *P. carterae* (CS-287), *T. lutea* [CS-177; original strain name *Isocrysis* sp. (Bendif *et al.*, 2013)], and the diatom, *Phaeodactylum tricornutum* (CS-29) were obtained from the Australian National Algae Culture Collection CSIRO (<https://www.csiro.au/en/Research/Collections/ANACC>) and grown at 20 °C in 0.2 µm filtered and autoclaved seawater containing f/2 (Guillard and Ryther, 1962) or GSe (*P. carterae*; Blackburn *et al.*, 2001) nutrients, vitamins, and trace metals. The cultures were

(A) Pyrenoid localization in the cell



(B) Evidence for CCM

CCM parameter	<i>P. lutheri</i>	<i>P. carterae</i>	<i>T. lutea</i> (<i>I. galbana</i>)	<i>P. tricornutum</i>
Pyrenoid	No	Yes (bulging)	Yes (immersed)	Yes (immersed)
Ci affinity affected by AZA or EZA	n.m.	AZA and EZA	EZA	EZA
CA activity stimulated in light	n.m.	n.m.	Yes	Yes
Cellular C_i pool increase	n.m.	n.m.	6 fold	5-6 fold
δ-CA detected	No	Yes	Yes	No

Fig. 2. Microalgae pyrenoid and CCM composition. (A) TEM images were compiled from the literature to represent the range of pyrenoids presented in this. To represent a pyrenoid lacking Pavlova, we use *Pavlova viridis* from Bendif *et al.* (2011) (Protist, 162, Bendif EM, Probert I, Hervé A, Billard C, Goux D, Lelong C, Cadoret JP, Véron B. Integrative taxonomy of the Pavlovophyceae (Haptophyta): a reassessment, 738–761, ©2011, with permission from Elsevier) as the TEM image clearly represents the lack of pyrenoid. *Pavlova lutheri* is visualized in the same study; however, the TEM image does not show the chloroplast (Ch) lacking a pyrenoid as clearly. TEM image of *P. carterae* from Beech and Wetherbee (1988) [republished with permission of the International Phycological Society from Observations on the flagellar apparatus and peripheral endoplasmic reticulum of the coccolithophorid, *Pleurochrysis carterae* (Prymnesiophyceae), Beech PL, Wetherbee R, Phycologia 27, 1988; permission conveyed through Copyright Clearance Center, Inc.] illustrates pyrenoids (Py) bulging toward the center of the cell, and the two species *T. lutea* (Bendif *et al.*, 2014) (Journal of Applied Phycology, Erratum to: On the description of *Tisochrysis lutea* gen. nov. sp. nov. and *Isocrysis nuda* sp. nov. in the Isochrysidales, and the transfer of *Dicrateria* to the Prymnesiales (Haptophyta), 26, 2014, 1617, Bendif EM, Probert I, Schroeder DC, de Vargas C. With permission of Springer) and *P. tricornutum* (Allen *et al.*, 2011) (Allen AE, Moustafa A, Montsant A, Eckert A, Kroth PG, Bowler C. Evolution and functional diversification of fructose bisphosphate aldolase genes in photosynthetic marine diatoms. Molecular Biology and Evolution 2012, 29, 367–279, by permission of Oxford University Press) show pyrenoids immersed within the chloroplast. (B) Summary of published experimental evidence for the presence of a CCM in the species with a pyrenoid. Evidence for a CCM is detectable by: (i) inhibition of CO_2 assimilation by the impermeable acetazolamide (AZA) or membrane-permeable ethoxzolamide (EZA) CA inhibitors (Burns and Beardall, 1987; Okazaki *et al.*, 1992; Badger *et al.*, 1998; Hopkinson *et al.*, 2013); (ii) stimulation of CA activity following cell illumination (Badger *et al.*, 1998); (iii) whether the intercellular C_i pool is higher than the external environment (Badger *et al.*, 1998); or (iv) the preliminary detection of δ-CA using methods described in the Materials and methods.

grown in polycarbonate culture flasks under $150 \pm 50 \mu\text{mol photons m}^{-2} \text{ s}^{-1}$ illumination on a 16:8 h light:dark cycle.

Pyrenoid morphology and CCM characterization.

Details of pyrenoid morphology and estimates of C_i and CA pools for the microalgae were compiled from the literature (Manton and Peterfi, 1969; Billard and Gayral, 1972; Green, 1975; Green and Pienaar, 1977; Borowitzka and Volcani, 1978; Hori and Green, 1985; Badger et al., 1998; Bendif et al., 2011, 2013). A preliminary screen for putative δ -CA genes was carried out using PCR. δ -CA is a functional carbonic anhydrase, as demonstrated *in vitro* by Del Prete et al. (2014) and Lee et al. (2013). It is regulated by CO_2 , and is thus important in inorganic carbon acquisition (Lane and Morel, 2000a).

Genomic DNA was extracted as described (Richlen and Barber, 2005) and candidate δ -CA genes were amplified by PCR using primers Δfwd (5'-GTTGGCGAGACGTACGAGGTGCACTGG-3') and Δrev (5'-GCGATCGACCTGCCAGGTGATGGG-3') that were designed to the conserved C-terminal amino acid sequences VGETYEVHW and PITWQVDR, respectively. The ~370 bp DNA product amplified from *P. carterae* and *Isochrysis galbana* (for comparison with *T. lutea*) was sequenced by Source BioScience (Oxford, UK). Confirmation that the absence of δ -CA from our *P. tricornutum* (strain CCAP1055/1 a monoclonal culture derived from a fusiform cell in May 2003 from strain CCMP632) was further supported by analysis for δ -CA homologs within the fully sequenced genome of *P. tricornutum* (Bowler et al., 2008) and its predicted protein products. Similarly, the absence of δ -CA was further confirmed by a search of the Pavlovales sp. CCMP2436 (JGI) genome sequence.

A BLAST search of the genomes was carried out using the δ -CA protein sequence from *Thalassiosira pseudonana* (BAO52718) and *Thalassiosira weissflogii* (AAV39532), both centric diatoms, and *Fragilariopsis cylindrus* CCMP1102 (OEU11320), a pennate diatom, as query sequences. The BLAST search yielded no hits. Together with our PCR, we concluded that there were no δ -CA homologs in this strain of *P. tricornutum*. A BLAST search was also carried out on the genome of Pavlovales sp. CCMP2436 (JGI), an environmental isolate using the δ -CA protein sequence from *T. pseudonana* (BAO52718) and the haptophytes *Emiliania huxleyi* (ABG37687), *I. galbana* (EC146202, EC142695), and *Chrysochromulina* sp. CCMP291 (KO021563, KO028292). Although this genome is not fully curated and the culture has not been taxonomically described, the preliminary search yielded no hits.

Rubisco extraction and kinetic assessment

Algal cells were harvested via centrifugation (2000 g for 10 min) and the pelleted cells snap-frozen in liquid nitrogen and stored at -80°C until assay. The crude soluble cell extracts were obtained by rupturing cells using a French press as described previously (Young et al., 2016). As detailed in the same study, Rubisco content was quantified by [^{14}C]CABP (2-carboxyarabinitol 1,5-bisphosphate) binding within the crude extract and concentrations of soluble protein were quantified using the Bradford assay against BSA. Rubisco catalytic parameters: maximum carboxylation rate ($k_{\text{cat}}^{\text{C}}$) and half-saturation constants for CO_2 and O_2 (K_{C} and K_{O} , respectively) were measured at 25°C using $^{14}\text{CO}_2$ fixation assays employing crude extract that had been activated for 10–15 min at 25°C with 10 mM MgCl_2 and 10 mM NaHCO_3 . The CO_2 concentrations in the $^{14}\text{CO}_2$ assays were calculated using the Henderson–Hasselbalch equation and the parameters detailed in (Sharwood et al., 2016a). Measurements of $S_{\text{C/O}}$ were made using Rubisco rapidly purified from ~1 g of pelleted algal cells as described (Young et al., 2016).

Simulating the influence of microalgae Rubisco on C_3 plant photosynthesis

The carboxylase activity-limited assimilation rates were simulated according to Farquhar et al. (1980) using the equation:

$$A = \frac{(C_c \cdot s_c - 0.5 \frac{s_c}{s_o}) k_{\text{cat}}^{\text{C}} \cdot B}{C_c \cdot s_c + K(1 + \frac{o}{K_o})} - R_d$$

assuming a CO_2 solubility in H_2O (s_c) of $0.0334 \text{ M bar}^{-1}$, an O of $267 \mu\text{M}$, a Rubisco content (B) of $20 \mu\text{mol catalytic sites m}^{-2}$, and a non-photorespiratory CO_2 assimilation rate (R_d) of $2 \mu\text{mol m}^{-2} \text{ s}^{-1}$. Under higher chloroplast CO_2 pressures (C_c), the photosynthetic rate becomes light- (or electron transport rate, ETR-) limited and is modeled according to the equation:

$$A = \frac{(C_c \cdot s_c - 0.5 \frac{s_c}{s_o})}{4(C_c \cdot s_c + \frac{o}{s_o})} - R_d$$

assuming an electron transport rate (J) of $150 \mu\text{mol m}^{-2} \text{ s}^{-1}$.

Results and Discussion

The differing pyrenoid morphologies within the microalgae studied

A central objective of this study was to examine the correlations between pyrenoid morphology, evidence of a CCM, and the content and catalysis of Rubisco in microalgae. As summarized in Fig. 2A, *T. lutea* possesses a pyrenoid immersed in the center of the plastid with 1–2 thylakoids traversing the center of the pyrenoid (Bendif et al., 2013; Borowitzka and Volcani, 1978). In contrast, the pyrenoid in *P. carterae* bulges out from the plastid toward the center of the cell, with 5–6 continuous thylakoids traversing the plastid and pyrenoid (Manton and Peterfi, 1969; Beech and Wetherbee, 1988). Immersed versus bulging pyrenoids differ in the location within the cell, relative separation from the plastid (i.e. the presence of a lipid membrane has been suggested from TEM observations), and the connectivity to plastid thylakoids. A lipid membrane has been observed around the immersed/semi-immersed pyrenoids of two other members of the Isochrysidales—*Chrysotila lamellosa* (Billard and Gayral, 1972; Green and Parke, 1975) and *Isochrysis galbana* (Green and Pienaar, 1977). However, Bendif et al. (2013) did not detect a membrane around the pyrenoid of *T. lutea* nor has one been observed around pyrenoids of the bulging morphotype in any haptophyte species, including *P. carterae*. In the Pavlovophyceae, the pyrenoids are often bulging towards the exterior of the cell—albeit not in *P. lutheri* where no pyrenoid is apparent (Green, 1975; Burris, 1981; Bendif et al., 2011). *Phaeodactylum tricornutum* was included in this study and, like many members of the lineage, has pyrenoids that are fully immersed within the chloroplast with 1–2 pyrenoid-traversing thylakoids (Borowitzka and Volcani, 1978; Bedoshvili et al., 2009) (Fig. 2A).

Experimental evidence for a CCM

A key component of a CCM is the enzyme CA that catalyzes the rapid interconversion between CO_2 and HCO_3^- . In marine primary producers, the CA activity of a CCM is particularly beneficial for accessing CO_2 from the high oceanic

HCO_3^- concentrations. The effects of two CA inhibitors, the membrane-permeable ethoxycarbonyl (EZA) and the relatively impermeable acetazolamide (AZA), are commonly used to test for CCM activity (Okazaki *et al.*, 1992). This is undertaken by examining the influence of EZA and AZA on the affinity of photosynthesis for plasma membrane-based inorganic carbon (C_i) (Okazaki *et al.*, 1992; Badger *et al.*, 1998) and light-stimulated CA activity (Burns and Beardall, 1987).

Using modern cell biology tools, there have been significant advances in understanding the CCM components in microalgae (Engel, 2015) which includes the discovery of novel CA isoforms and their intercellular localization (Jin *et al.*, 2016; Kikutani *et al.*, 2016). While a comparable detailed analysis of haptophyte CCM components is beyond the scope of this work, Fig. 2B summarizes the known CCM features in the microalgae studied here. EZA treatment reduces the affinity for C_i in photosynthesis for the pyrenoid-containing *I. galbana* (as a proxy for *T. lutea*), *P. tricornutum*, and *P. carterae* species, with the external CA inhibitor AZA also affecting the C_i affinity in *P. carterae* (Badger *et al.*, 1998; Chen *et al.*, 2006; Hopkinson *et al.*, 2013). We note that other diatoms with fully immersed pyrenoids have been shown to be sensitive to AZA (Hopkinson *et al.*, 2013). The influence of EZA or AZA on the photosynthetic carbon assimilation rate in *P. lutheri*, the species lacking a pyrenoid, remains untested. Similarly, the light-stimulated CA activity found in *P. tricornutum* and *T. lutea* has yet to be examined in *P. carterae* and *P. lutheri* (Fig. 2B). It is estimated that the CCMs associated with immersed pyrenoids can increase intracellular C_i pools ~6-fold higher than that permissible by passive diffusion (Fig. 2B (Burns and Beardall, 1987; Colman and Rotatore, 1995; Badger *et al.*, 1998).

The δ isoform of CA (or TWCA1), whose expression in the diatom *T. weissflogii* is modulated by extracellular CO_2 levels (Morel *et al.*, 1994; Lane and Morel, 2000a, b) and in marine dinoflagellates functions as an external CA (Lapointe *et al.*, 2008), holds the potential as a key component of a CCM in microalgae. The catalytic activity and inhibition of δ -CA demonstrate the functionality of the CA in the diatom *Thalassiosira pseudonana* and the haptophyte *Emiliania huxleyi* (Soto *et al.*, 2006; Lee *et al.*, 2013; Del Prete *et al.*, 2014). Using sequence homology searches, we were able to detect δ -CA homologs in genome data sets for *P. carterae* and *T. lutea*, but not in *P. tricornutum* or *P. lutheri* (using the Pavlova sp. CCMP2436 genome as a proxy). Importantly the absence of detectable sequence homology does not disqualify these microalgae from producing δ -CA or alternative CA isoforms, especially considering that new CAs are still being discovered (Jin *et al.*, 2016; Kitkanti *et al.*, 2016). Indeed, a number of other CA types are expressed in *P. tricornutum* that include one localized in the pyrenoid (Tachibana *et al.*, 2011), an extracellular CA (Hopkinson *et al.*, 2013), and a θ -type CA located in the thylakoid lumen (Jin *et al.*, 2016). Our BLAST search of the Pavlova sp. CCMP2436 genome supports the absence of a δ -CA in *P. lutheri*; however, further investigation is required (e.g. whether *P. lutheri* contains other forms of CA). Overall, the existing evidence suggests that the presence

of a pyrenoid coincides with the presence and activity of CA (Fig. 2B), consistent with their role in the microalgae CCM.

The carboxylation properties of haptophyte Rubisco

Form 1B Rubisco from organisms operating a CCM characteristically show higher rates of maximum carboxylation $k_{\text{cat}}^{\text{C}}$ and a reduction in CO_2 affinity (i.e. an increase in K_{C}) than the Rubisco from their non-CCM relatives. For example, the Rubisco from C_4 plants typically have a higher $k_{\text{cat}}^{\text{C}}$ and higher K_{C} than C_3 plant Rubisco (Sage, 2002; Savir *et al.*, 2010; Sharwood *et al.*, 2016a, c; Tcherkez, 2016). As shown in Fig. 3A, the K_{C} diversity among Form 1B vascular plant Rubisco spans a limited range in values relative to the Form 1D Rubisco from diatoms (Hanson, 2016; Young *et al.*, 2016). Moreover, the relationship between K_{C} and $k_{\text{cat}}^{\text{C}}$ at 25 °C for the Form 1D Rubisco differs from Form 1B Rubisco (Fig. 3A).

For comparison of different CCM effectiveness on Rubisco kinetics within organisms containing the 1D Rubisco, we examined the kinetics of the Form 1D Rubiscos from freshly lysed *P. carterae*, *T. lutea*, and *P. lutheri* cells. The Rubisco activity in the cellular extract was stable at 25 °C for at least 20 min following extraction (see Supplementary Fig. S1 at JXB online). The CO_2 - Mg^{2+} activation status of the extracted Rubisco varied between 50% and 60%, comparable with that seen in the cellular extract of diatoms (Young *et al.*, 2016). To ensure full activation of all eight catalytic sites in each L_8S_8 molecule, the cellular extract was incubated for 10–15 min at 25 °C in buffer containing 10 mM MgCl_2 and 10 mM NaHCO_3 before assaying $k_{\text{cat}}^{\text{C}}$ under varying CO_2 concentrations by $^{14}\text{CO}_2$ fixation. By this approach, the values of $k_{\text{cat}}^{\text{C}}$ and K_{C} extrapolated from fitting the data to the Michaelis–Menten equation were reproducible between replicate cellular preparations (Table 1).

Significant kinetic diversity at 25 °C was observed among each haptophyte Rubisco relative to *P. tricornutum* (model diatom species) and *Nicotiana tabacum* (tobacco, model plant Rubisco used in kinetic comparisons; Whitney *et al.*, 2001; Sharwood *et al.*, 2016a, b) (Table 1). The $k_{\text{cat}}^{\text{C}}$ of *P. carterae*, *P. tricornutum*, and tobacco were similar and each ~50% higher than those of *T. lutea* and *P. lutheri* Rubisco. Comparable levels of variation in K_{C} were also observed among the haptophyte Rubiscos (14.5–24.1 μM) that are notably lower and spanning a smaller range than the K_{C} values of diatom Rubiscos (22–70 μM ; Fig. 3A). This suggests haptophyte Rubisco may experience a lower CO_2 microenvironment relative to diatoms. This is probably the case for Rubisco in *P. lutheri* that lacks a pyrenoid (Burris, 1981; Bendif *et al.*, 2011) and whose Rubisco has the lowest K_{C} and highest $S_{\text{C/O}}$ (i.e. a greater selectivity for CO_2 over O_2 ; Table 1).

A correlative analysis of haptophyte Rubisco kinetics

A comparison of Rubisco kinetics of each haptophyte identified contrasting relationships when compared with the 25 °C properties of Form 1B and 1D L_8S_8 Rubisco from a range of eukaryotic phototrophs (Fig. 3A–E; data compiled in

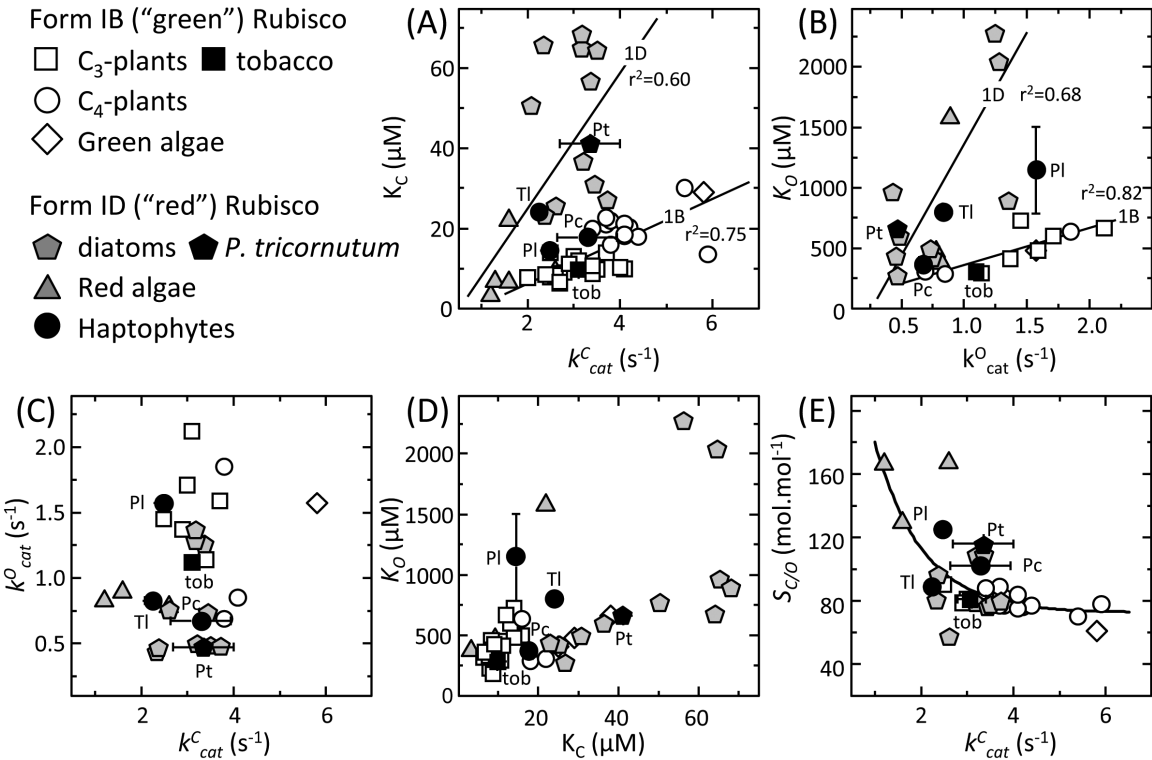


Fig. 3. The diversity in the kinetic properties of haptophyte Rubisco at 25 °C. Comparative relationships between the kinetic properties measured in this study for Rubisco from *P. lutheri* (Pl), *P. carterae* (Pc), *T. lutea* (Tl), the diatom *P. tricornutum* (Pt), and from tobacco (Tob) with those of other Form 1B and 1D Rubiscos (see key) as curated by Young et al. (2016). The plotted maximal carboxylation and oxygenation turnover rates (k_{cat}^C , k_{cat}^O), relative specificity for CO₂ over O₂ ($S_{C/O}$), and the Michaelis constants (K_m) for CO₂ and O₂ (K_C , K_O) are from Table 1. Linear regressions are shown for the differing (A) k_{cat}^C – K_C and (B) k_{cat}^O – K_O relationships displayed for Form 1B and 1D Rubiscos. No statistically significant relationships were evident among correlative analyses of (C) k_{cat}^C and k_{cat}^O , K_C or between (D) K_C and K_O . (E) An exponential relationship was apparent when comparing the kinetic trade-off between $S_{C/O}$ with k_{cat}^C with the differing phylogenetic Rubisco groupings aggregated at differing positions along the gradient

Table 1. Rubisco kinetic parameters measured at 25 °C

Species	k_{cat}^C (s ⁻¹)	K_C (μM)	K_O (μM)	$S_{C/O}$ (mol mol ⁻¹)	$K_C^{21\% O_2}$ (μM)	k_{cat}^O (s ⁻¹)	k_{cat}^O/K_O (mM ⁻¹ s ⁻¹)	CE	
								k_{cat}^C/K_C (mM ⁻¹ s ⁻¹)	$k_{cat}^C K_C^{21\%O_2}$ (mM ⁻¹ s ⁻¹)
Haptophytes									
<i>P. carterae</i>	3.3 ± 0.4	17.7 ± 1.5	366 ± 60	102 ± 1	30.6	0.7	1.8	186	108
<i>T. lutea</i>	2.2 ± 0.1	24.1 ± 0.5	800 ± 55	89 ± 1	32.2	0.8	1.0	91	68
<i>P. lutheri</i>	2.5 ± 0.1	14.5 ± 1.6	1146 ± 212	125 ± 2	17.8	1.6	1.4	172	140
Diatom ^a									
<i>P. tricornutum</i>	3.3 ± 0.5	41.1 ± 1.3	664 ± 54	116 ± 2	57.6	0.5	0.7	80	55
C ₃ plant ^a									
<i>N. tabacum</i>	3.1 ± 0.3	9.7 ± 0.1	283 ± 15	81 ± 1	18.9	1.1	3.9	319	164

CE, carboxylation efficiency.
The rate of oxygenation (k_{cat}^O) was calculated using the equation $k_{cat}^O = (k_{cat}^C \times K_O) / (K_C \times S_{C/O}) \times K_C$ at 25 °C under ambient atmospheric O₂ levels; $K_C^{21\%O_2}$ was calculated as $K_C(1 + [O_2]/K_O)$ assuming an O₂ solubility of 0.00126 mol (l bar)⁻¹ and an atmospheric pressure of 1.013 bar resulting in an [O₂] value of 267 μM in solution.
Values shown are average of measurements from $n \geq 3$ (±SD) biological repeat samples.
^aData from Young et al. (2016).

Supplementary Table S1). An examination of the K_C – k_{cat}^C relationship for ‘green’ Form 1B (vascular plants, CCM-positive green algae) and ‘non-green’ Form 1D (diatoms, haptophytes, and red algae) Rubisco suggests they follow differing trajectories (Fig. 3A). As suggested previously, this might arise from lineage-dependent variation in ribulose

bisphosphate (RuBP) enolization energies and/or mechanistic differences in their multistep carboxylation chemistry (Tcherkez, 2013, 2016; Young et al., 2016).
With regard to haptophyte Rubisco, the K_C – k_{cat}^C relationship of *P. lutheri* and *P. carterae* Rubisco appeared to align more closely with Form 1B Rubisco (Fig. 3A). Consequently,

their carboxylation efficiencies under both anaerobic ($k_{\text{cat}}^{\text{C}}/K_{\text{C}}$) and ambient O_2 ($k_{\text{cat}}^{\text{C}}/K_{\text{C}}^{21\%\text{O}_2}$) are higher than those of *T. lutea* Rubisco (Table 1) whose $K_{\text{C}}-k_{\text{cat}}^{\text{C}}$ relationship closely aligns with red algae and diatom Form 1D Rubiscos (Fig. 3A), and lower carboxylation efficiency of *P. tricornutum* Rubisco (Table 1). These findings suggest that there may be differences in the CCM effectiveness between the bulging pyrenoids in *P. carterae* relative to the immersed pyrenoids of diatoms and *T. lutea*. It also raises questions regarding how differences in the CCM and/or cellular metabolism in phytoplankton with immersed pyrenoids have led to the evolution of atypical Form 1D Rubisco kinetics.

Somewhat analogous to their differing $K_{\text{C}}-k_{\text{cat}}^{\text{C}}$ relationships, both Form 1B and 1D enzymes showed differing linear correlations between K_{O} and $k_{\text{cat}}^{\text{O}}$ (Fig. 3B) but no identifiable correlations between their $k_{\text{cat}}^{\text{C}}/k_{\text{cat}}^{\text{O}}$ (Fig. 3C) and $K_{\text{C}}/K_{\text{O}}$ (Fig. 3D) relationships. This finding is consistent with increasing experimental evidence that changes in the carboxylation and oxygenation properties are not coupled in an obligatory manner (Savir *et al.*, 2010; Whitney *et al.*, 2011; Sharwood *et al.*, 2016a; Sharwood, 2017). This unfastening of carboxylation and oxygenation has enabled significant Rubisco kinetic diversity to have evolved in nature, in particular with regard to CO_2/O_2 selectivity ($S_{\text{C/O}}$) whose correlative trade-off with $k_{\text{cat}}^{\text{C}}$ follows a diffuse exponential relationship (Fig. 3E; Sharwood, 2017) rather than the linear response previously postulated (Tcherkez *et al.*, 2006; Savir *et al.*, 2010). Within the $k_{\text{cat}}^{\text{C}}-S_{\text{C/O}}$ relationship, the haptophyte Rubisco localizes in a region comparable with diatom Rubisco between the high $S_{\text{C/O}}$, low $k_{\text{cat}}^{\text{C}}$ of Form 1D red algae Rubisco and the lower $S_{\text{C/O}}$, higher $k_{\text{cat}}^{\text{C}}$ of Form 1B Rubisco (Fig. 3E).

Interpreting the differing O_2 sensitivities of haptophyte Rubisco

While the CCMs of phototrophic organisms function to elevate the $\text{CO}_2:\text{O}_2$ ratio around Rubisco through increased CO_2 supply, it is unclear how the ratio is dependent on complementary mechanisms to lower O_2 . In many organisms employing a CCM, the O_2 -generating components are located away from Rubisco. For example, the Rubisco-containing bundle sheath cell (BSC) chloroplasts in C_4 plants within NADP-malic enzyme (NADP-ME) subtypes characteristically lack the O_2 -evolving PSII complexes (Sage *et al.*, 2014; von Caemmerer and Furbank, 2016). Similarly, the thylakoids traversing the pyrenoid of the red algae *Porphyridium cruentum* lack PSII (McKay and Gibbs, 1990), while in the dinoflagellate *Gonyaulax polyedra* during times of high carbon fixation the Rubisco is spatially relocated to pyrenoids near the cell center away from the O_2 -evolving light-harvesting reactions (Nassoury *et al.*, 2001). Similarly in cyanobacteria, the carboxysomes localize to the cell interior away from the PSII thylakoids lining the cell periphery (Liberton *et al.*, 2011). These strategies for spatially separating O_2 production away from Rubisco appear to be key components of the CCM. Unfortunately, measuring the O_2 concentration in bundle sheath cell chloroplasts, cyanobacteria carboxysomes, or inside the pyrenoid of algae remains an insurmountable challenge.

As indicated above, the oxygenation properties of Rubisco show significant natural variation. Drawing correlations between their O_2 sensitivity (i.e. K_{O}) and CCM efficiency is therefore quite challenging. An additional complexity is that the extent of O_2 solubility is reduced by the highly proteinaceous matrix of pyrenoids, chloroplasts, and carboxysomes (Tcherkez, 2016) and by the increasing pressures experienced by microalgae down the water column. Interestingly the higher K_{O} of *T. lutea*, *P. tricornutum*, and *P. lutheri* Rubisco lend to limiting the influence of changing O_2 concentrations on carboxylation efficiency relative to Rubisco from tobacco and *P. carterae* (Fig. 4). This implies that the variable O_2 concentrations experienced by diatoms and haptophytes within the water column might have influenced their Rubisco kinetic evolution. Furthermore, pyrenoid morphology and ultrastructure may also have influenced the evolved oxygenase properties. For example, *P. lutheri* Rubisco exhibits a low affinity for O_2 ($K_{\text{O}} \sim 1150 \mu\text{M}$), implying that its Rubisco experiences higher O_2 concentrations than the Rubisco from algae possessing immersed (e.g. *T. lutea*, *P. tricornutum*, $K_{\text{O}} \sim 650\text{--}800 \mu\text{M}$) or bulging (*P. carterae*, $K_{\text{O}} \sim 366 \mu\text{M}$) pyrenoids (Table 1).

These observations could be interpreted to suggest that the pyrenoids, in particular those with a bulging morphology, might be lowering the O_2 environment to augment the $\text{CO}_2:\text{O}_2$ ratio around Rubisco. Possibly internally bulging pyrenoids may locate Rubisco closer to the reducing chemistry of the cytosol or the mitochondria and their respired CO_2 . Other mechanisms for altering pyrenoid $\text{CO}_2:\text{O}_2$ include reducing thylakoid number within the pyrenoid, reducing the O_2 -producing PSII activity (McKay and Gibbs, 1990), or employing pyrenoid tubules for diffusion (Engel *et al.*, 2015). Challenging these hypotheses is the observed high K_{O} ($\sim 2000 \mu\text{M}$, indicating an insensitivity to O_2) for Rubisco

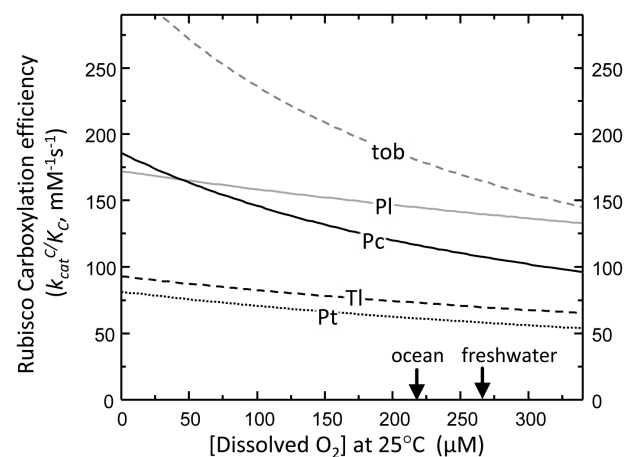


Fig. 4. The differential effect of O_2 on Rubisco carboxylation efficiency. Variation in the response of carboxylation efficiency (CE; $k_{\text{cat}}^{\text{C}}/K_{\text{C}}$) to O_2 levels (O) for Rubisco from tobacco (tob, vascular plant control), the diatom *P. tricornutum* (Pt, dotted line), and the haptophytes *P. lutheri* (Pl, solid gray line), *P. carterae* (Pc, solid black line), and *T. lutea* (Tl, dashed black line). Lines were fitted to the equation $\text{CE} = k_{\text{cat}}^{\text{C}}/[K_{\text{C}} \times (1 + (\text{O}/K_{\text{O}}))]$ using the parameters listed in Table 1. Arrows indicate the differing O_2 levels in fresh water and the ocean surface [assuming $\sim 3.5\%$ (w/v) salinity] at an atmospheric pressure of 1.013 bar.

from the pyrenoid-containing diatom *Thalassiosira weissflogii* (Young et al., 2016) and that multiple thylakoids traverse the pyrenoid of *P. carterae*, albeit with untested levels of PSII activity (Manton and Peterfi, 1969).

The influence of a CCM on the Rubisco requirement in haptophytes

A characteristic feature of the CCM in C_4 plants is that it reduces the requirement for Rubisco, allowing for increased nitrogen use efficiency (Ghannoum et al., 2005). In diatoms, the Rubisco content was found to correlate with K_C , suggesting that the allocation of resources into the enzyme may depend on CCM efficiency (Young et al., 2016). For example, the low K_C of Rubisco from *Phaeodactylum* and *Chaetoceros* diatom species correlated with increased investment in Rubisco content, while in *Thalassiosira* and *Skeletonema* species it was hypothesized that resources were instead allocated to the CCM rather than Rubisco to saturate the enzymes low CO_2 affinity (Young et al., 2016).

Among the three haptophyte species examined here, we identified a negative relationship between increasing CO_2 affinity (i.e. reducing K_C) and increasing Rubisco content (dashed line, Fig. 5). The trajectory of this relationship poorly correlated with the Rubisco content and K_C of *P. tricornutum*. While it is known that Rubisco content in diatoms can be influenced by growth stage (Losh et al., 2013), our measurements comprised replicate algae samples from cultures growing under non-nutrient limiting conditions and resulted in reproducible measures of Rubisco content (Fig. 5). While future experiments are aimed at examining these properties from a wider range of microalgae species, it is apparent that in the pyrenoid-lacking *P. lutheri* cells there is ~3- to 4-fold higher investment of soluble cellular protein in Rubisco (Fig. 5). Likewise, the Rubisco content in horn-works also shows a comparable correlation with the presence/

absence of pyrenoids (Hanson et al., 2002). Similarly, in C_3 plants, Rubisco comprises a larger resource investment [25–50% (w/w) total soluble protein] relative to C_4 plants where the CCM and higher k_{cat}^C reduces the amount of Rubisco required [i.e. 8–15% (w/w) of the soluble cellular protein (Ghannoum et al., 2005; Sharwood et al., 2016a, c)].

How suited is phytoplankton Rubisco to supporting photosynthesis in C_3 plants?

Improving the catalytic efficiency of Rubisco is a key target for improving the rate of photosynthesis and growth in key C_3 crops such as rice and wheat (Long et al., 2015; Sharwood et al., 2016b). This has led to considerable interest in identifying whether the natural catalytic diversity of Rubisco can be exploited to deliver improvements in crop Rubisco performance. The faster Rubisco from *Synechococcus* PCC7942 (cyanobacteria) and the photosynthetic bacterium *Rhodospirillum rubrum* are not able to support faster C_3 plant growth, even under elevated CO_2 , due to their low carboxylation efficiencies under ambient O_2 ($k_{cat}^C/K_C^{21\%O_2}$) and their low $S_{C/O}$ (Sharwood, 2017). In comparison, the higher $k_{cat}^C/K_C^{21\%O_2}$ and $S_{C/O}$ of the Form 1D Rubisco from *Griffithsia monilis* (filamentous red algae) would support faster rates of photosynthesis in C_3 crops with the potential to improve productivity by up to 30% (Long et al., 2015). Realizing this benefit is impeded by the incompatible assembly requirements of Form 1D Rubisco in plant chloroplasts (Whitney et al., 2001). Nevertheless, it is hoped solutions to improving crop Rubisco may be achieved through increased understanding of natural kinetic diversity among all Rubisco

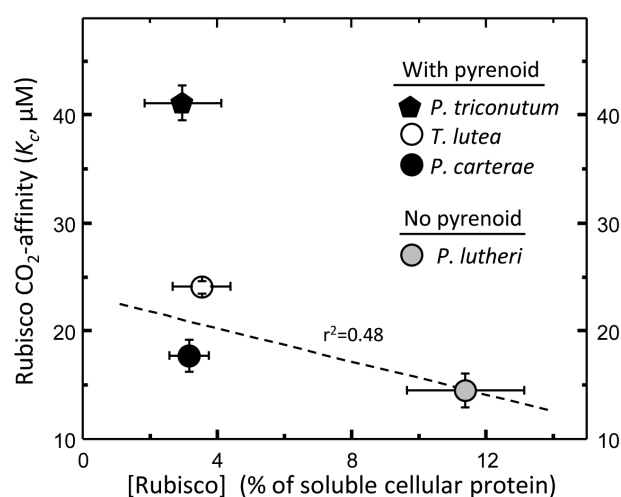


Fig. 5. Rubisco content is reduced in pyrenoid-containing phytoplankton. The Rubisco content (quantified by [^{14}C]CABP binding and expressed as a percentage of the cellular soluble protein) in cells grown at 20 °C under saturating nutrients was higher ($11.4 \pm 1.2\%$) in the pyrenoid-lacking *P. lutheri* cells relative to that in *P. carterae* ($3.0 \pm 0.8\%$), *T. lutea* ($3.5 \pm 0.9\%$), and *P. tricornutum* ($3.2 \pm 0.6\%$).

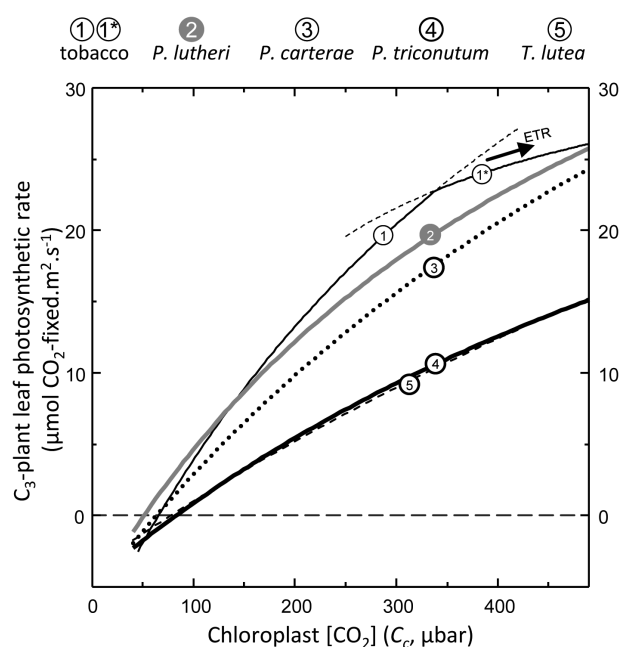


Fig. 6. The varying potential of phytoplankton Rubisco in a C_3 leaf. The influence of each Rubisco analyzed in Table 1 on CO_2 assimilation rates (A) at 25 °C in a C_3 leaf as a function of C_c was modeled according to Farquhar et al. (1980) as described in the Materials and methods. For the tobacco Rubisco, the photosynthetic rate became light limited (indicated by 1*) at $C_c > 320 \mu bar$.

forms (Whitney *et al.*, 2011; Sharwood, 2017). We therefore used the modeling approach of Farquhar *et al.* (1980) to simulate how each microalga would influence C_3 photosynthesis under varying chloroplast CO_2 concentrations (C_c ; Fig. 6). The low $k_{cat}^C/K_C^{21\%O_2}$ of *T. lutea* (and *P. tricornutum*) Rubisco (Table 1) impeded their simulated effect on C_3 photosynthesis at 25 °C. In contrast, the high $S_{C/O}$ of *P. lutheri* Rubisco improved the simulated photosynthetic rates relative to tobacco Rubisco under low C_c but not above 150 μ bar of CO_2 due to its lower k_{cat}^C and $k_{cat}^C/K_C^{21\%O_2}$ (Table 1). This finding suggests that future kinetic surveys to identify microalgae Rubisco better suited to operating in C_3 plant chloroplasts might best focus on microalgae that lack a pyrenoid and a CCM.

Conclusions and future directions

Due to their importance at the base of the marine food chain, global biogeochemical cycling, and interpretation of paleo-chemical signals in marine sediments, it is essential that we better understand the diversity and function of the algae CCMs. In this pilot study, we provide preliminary evidence for correlations between Rubisco content, kinetics, and pyrenoid morphology within the chloroplast of different haptophytes and the diatom *P. tricornutum*. Recent work has highlighted the lack of knowledge on the components and variable efficiency of the CCM across environmentally important microalgae (Hanson, 2016; Hopkinson *et al.*, 2016; Young *et al.*, 2016). Previous models of the algal CCM relied on correlations with distant photosynthetic organisms and limited Rubisco kinetic data. Elucidating the diversity and biological relevance of CCMs in these species will provide the groundwork necessary for understanding primary production in the world's oceans.

Our study provides evidence for the potential to use the binding affinities of Rubisco as a probe to gauge the intracellular $CO_2:O_2$ ratio around Rubisco and which might include an oxygen exclusion function by the pyrenoid. Future correlative analyses of Form 1D and Form 1B Rubisco kinetics from microalgae lacking pyrenoids and with differing pyrenoid morphologies are needed to yield a more robust functional understanding of the intrapyrenoid microenvironment and the natural diversity in carbon fixation in both terrestrial and aquatic ecosystems. Although challenging to measure, these Rubisco analyses are essential for understanding both (i) the different evolutionary histories of Form I Rubisco whose kinetics appear to have divergently evolved and (ii) the extent to which the competing carboxylation and oxygenation properties can be decoupled. Refining the existing assumptions about diversity and trends in photosynthetic evolution are paramount. Included in such endeavors are whether the non-canonical correlation between K_C and k_{cat}^C is limited to Form 1D Rubisco from microalgae with immersed pyrenoids (Fig. 3A), if resource allocation to Rubisco is elevated in species with a less effective CCM (Fig. 5), and to what extent increases in $k_{cat}^C/K_C^{21\%O_2}$, $S_{C/O}$, and K_O (i.e. a reduced O_2 sensitivity) can be used as a proxy to gauge the effectiveness of microalgae CCMs.

Supplementary data

Supplementary data are available at *JXB* online.

Fig. S1. Measurement of Rubisco activation status and stability *in vitro* at 25 °C.

Table S1. Rubisco kinetics at 25 °C as shown in Fig. 3.

Acknowledgements

AMCH was funded through a Clarendon Scholarship, Oxford and ANU visiting scholar (CE140100015). Funding for JNY and SMW was provided through Australian Research Council Grant CE14010001. RES was funded through the ARC DECRA scheme (DE13010760) and REMR was funded through an ERC Starting Grant (SP2-GA-2008-200915).

References

- Allen AE, Moustafa A, Montsant A, Eckert A, Kroth PG, Bowler C. 2012. Evolution and functional diversification of fructose biphosphate aldolase genes in photosynthetic marine diatoms. *Molecular Biology and Evolution* **29**, 367–279.
- Badger MR, Andrews TJ, Whitney SM, Ludwig M, Yellowlees DC, Leggat W, Price GD. 1998. The diversity and coevolution of Rubisco, plastids, pyrenoids, and chloroplast-based. *Canadian Journal of Botany* **1071**, 1052–1071.
- Badger MR, Hanson D, Price GD. 2002. Evolution and diversity of CO_2 concentrating mechanisms in cyanobacteria. *Functional Plant Biology* **29**, 161–173.
- Bedoshvili YD, Popkova TP, Likhoshvay YV. 2009. Chloroplast structure of diatoms of different classes. *Cell and Tissue Biology* **3**, 297–310.
- Beech PL, Wetherbee R. 1988. Observations on the flagellar apparatus and peripheral endoplasmic reticulum of the coccolithophorid, *Pleurochrysis carterae* (Prymnesiophyceae). *Phycologia* **27**, 142–158.
- Bendif EM, Probert I, Hervé A, Billard C, Goux D, Lelong C, Cadoret JP, Véron B. 2011. Integrative taxonomy of the Pavlovophyceae (Haptophyta): a reassessment. *Protist* **162**, 738–761.
- Bendif EM, Probert I, Schroeder DC, de Vargas C. 2013. On the description of *Tisochrysis lutea* gen. nov. sp. nov. and *Isochrysis nuda* sp. nov. in the Isochrysidales, and the transfer of *Dicrateria* to the Prymnesiales (Haptophyta). *Journal of Applied Phycology* **25**, 1763–1776.
- Bendif EM, Probert I, Schroeder DC, de Vargas C. 2014. Erratum to: On the description of *Tisochrysis lutea* gen. nov. sp. nov. and *Isochrysis nuda* sp. nov. in the Isochrysidales, and the transfer of *Dicrateria* to the Prymnesiales (Haptophyta). *Journal of Applied Phycology* **26**, 1617.
- Berner RA. 2006. GEOCARBSULF: a combined model for Phanerozoic atmospheric O_2 and CO_2 . *Geochimica et Cosmochimica Acta* **70**, 5653–5664.
- Berner RA, Canfield DE. 1989. A new model for atmospheric oxygen over Phanerozoic time. *American Journal of Science* **289**, 333–361.
- Billard C, Gayral P. 1972. Two new species of *Isochrysis* with remarks on the genus *Ruttnera*. *British Phycological Journal* **7**, 289–297.
- Blackburn SI, Bolch CJS, Haskard KA, Hallegraeff GM. 2001. Reproductive compatibility among four global populations of the toxic dinoflagellate *Gymnodinium catenatum* (Dinophyceae). *Phycologia* **40**, 78–87.
- Borowitzka MA, Volcani BE. 1978. The polymorphic diatom *Phaeodactylum tricornutum*: ultrastructure of its morphotypes. *Journal of Phycology* **14**, 10–21.
- Bowler C, Allen AE, Badger JH, *et al.* 2008. The *Phaeodactylum* genome reveals the evolutionary history of diatom genomes. *Nature* **456**, 239–244.
- Burns BD, Beardall J. 1987. Utilization of inorganic carbon by marine microalgae. *Journal of Experimental Marine Biology and Ecology* **107**, 75–86.
- Burris JE. 1981. Effects of oxygen and inorganic carbon concentrations on the photosynthetic quotients of marine algae. *Marine Biology* **65**, 215–219.

- Canfield DE.** 2005. The early history of atmospheric oxygen: homage to Robert M. Garrels. *Annual Review of Earth and Planetary Sciences* **33**, 1–36.
- Chen X, Qiu CE, Shao JZ.** 2006. Evidence for K⁺-dependent HCO₃[−] utilization in the marine diatom *Phaeodactylum tricornutum*. *Plant Physiology* **141**, 731–736.
- Colman B, Rotatore C.** 1995. Photosynthetic inorganic carbon uptake and accumulation in two marine diatoms. *Plant, Cell and Environment* **18**, 919–924.
- Del Prete S, Vullo D, De Luca V, Supuran CT, Capasso C.** 2014. Biochemical characterization of the δ-carbonic anhydrase from the marine diatom *Thalassiosira weissflogii*, TweCA. *Journal of Enzyme Inhibition and Medicinal Chemistry* **29**, 906–911.
- Engel BD, Schaffer M, Kuhn Cuellar L, Villa E, Plitzko JM, Baumeister W.** 2015. Native architecture of the *Chlamydomonas* chloroplast revealed by in situ cryo-electron tomography. *eLife* **4**, e04889.
- Farquhar GD, von Caemmerer S, Berry JA.** 1980. A biochemical model of photosynthetic CO₂ assimilation in leaves of C₃ species. *Planta* **149**, 78–90.
- Ghannoum O, Evans JR, Chow WS, Andrews TJ, Conroy JP, von Caemmerer S.** 2005. Faster Rubisco is the key to superior nitrogen-use efficiency in NADP-malic enzyme relative to NAD-malic enzyme C4 grasses. *Plant Physiology* **137**, 638–650.
- Green JC.** 1975. The fine structure and taxonomy of the haptophycean flagellate *Pavlova lutheri* (Droop) comb. nov. *Journal of the Marine Biological Association UK* **55**, 785–793.
- Green JC, Parke M.** 1975. New observations upon members of the genus *Chrysotila* Anaand, with remarks upon their relationship within the Haptophyceae. *Journal of the Marine Biological Association of the United Kingdom* **50**, 1125–1136.
- Green JC, Pienaar RN.** 1977. The taxonomy of the order Isocrysidales (Prymnesiophyceae) with special reference to the genera *Isocrysis* Parke, *Dicrateria* Parke and *Imantonia* Reynolds. *Journal of the Marine Biological Association UK* **57**, 7–17.
- Guillard RR, Ryther JH.** 1962. Studies of marine planktonic diatoms. I. *Cyclotella nana* Hustedt, and *Detonula confervacea* (Cleve) Gran. *Canadian Journal of Microbiology* **8**, 229–239.
- Hanson DT.** 2016. Breaking the rules of Rubisco catalysis. *Journal of Experimental Botany* **67**, 3180–3182.
- Hanson D, Andrews TJ, Badger MR.** 2002. Variability of the pyrenoid-based CO₂ concentrating mechanisms in hornworts (Anthocerotophyta). *Functional Plant Biology* **29**, 407–416.
- Hopkinson BM, Dupont CL, Allen AE, Morel FMM.** 2011. Efficiency of the CO₂-concentrating mechanism of diatoms. *Proceedings of the National Academy of Sciences, USA* **108**, 3830–3837.
- Hopkinson BM, Dupont CL, Matsuda Y.** 2016. The physiology and genetics of CO₂ concentrating mechanisms in model diatoms. *Current Opinion in Plant Biology* **31**, 51–57.
- Hopkinson BM, Meile C, Shen C.** 2013. Quantification of extracellular carbonic anhydrase activity in two marine diatoms and investigation of its role. *Plant Physiology* **162**, 1142–1152.
- Hori T, Green JC.** 1985. The ultrastructure of mitosis in *Isochrysis galbana* Parke (Prymnesiophyceae). *Protoplasma* **125**, 140–151.
- Hovde BT, Deodato CR, Hunsperger HM, et al.** 2015. Genome sequence and transcriptome analyses of *Chrysochromulina tobin*: metabolic tools for enhanced algal fitness in the prominent order Prymnesiales (Haptophyceae). *PLoS Genetics* **11**, e1005469.
- Jin S, Sun J, Wunder T, Tang D, Cousins AB, Sze SK, Mueller-Cajar O, Gao Y-G.** 2016. Structural insights into the LCIB protein family reveals a new group of β-carbonic anhydrases. *Proceedings of the National Academy of Sciences, USA* **113**, 14716–14721.
- Karlsson J, Clarke AK, Chen ZY, Huggins SY, Park YI, Husic HD, Moroney JV, Samuelsson G.** 1998. A novel alpha-type carbonic anhydrase associated with the thylakoid membrane in *Chlamydomonas reinhardtii* is required for growth at ambient CO₂. *EMBO Journal* **17**, 1208–1216.
- Kikutani S, Nakajima K, Nagasato C, Tsuji Y, Miyatake A, Matsuda Y.** 2016. Thylakoid luminal θ-carbonic anhydrase critical for growth and photosynthesis in the marine diatom *Phaeodactylum tricornutum*. *Proceedings of the National Academy of Sciences, USA* **113**, 9828–9833.
- Lane TW, Morel FM.** 2000a. Regulation of carbonic anhydrase expression by zinc, cobalt, and carbon dioxide in the marine diatom *Thalassiosira weissflogii*. *Plant Physiology* **123**, 345–352.
- Lane TW, Morel FMM.** 2000b. A biological function for cadmium in marine diatoms. *Proceedings of the National Academy of Sciences, USA* **97**, 4627–4631.
- Lapointe M, Mackenzie TD, Morse D.** 2008. An external delta-carbonic anhydrase in a free-living marine dinoflagellate may circumvent diffusion-limited carbon acquisition. *Plant Physiology* **147**, 1427–1436.
- Lara MAV, Andreo CS.** 2011. C₄ plants adaptation to high levels of CO₂ and to drought environments. In: **Shanker A**, ed. *Plants—mechanisms and adaptations*. InTech, 415–428.
- Lee RB, Smith JA, Rickaby RE.** 2013. Cloning, expression and characterization of the δ-carbonic anhydrase of *Thalassiosira weissflogii* (Bacillariophyceae). *Journal of Phycology* **49**, 170–177.
- Liberton M, Austin JR 2nd, Berg RH, Pakrasi HB.** 2011. Insights into the complex 3-D architecture of thylakoid membranes in unicellular cyanobacterium *Cyanothece* sp. ATCC 51142. *Plant Signaling and Behavior* **6**, 566–569.
- Liu H, Aris-Brosou S, Probert I, de Vargas C.** 2010. A time line of the environmental genetics of the haptophytes. *Molecular Biology and Evolution* **27**, 161–176.
- Loganathan N, Tsai Y-CC, Mueller-Cajar O.** 2016. Characterization of the heterooligomeric red-type rubisco activase from red algae. *Proceedings of the National Academy of Sciences, USA* **113**, 14019–14024.
- Long SP, Marshall-Colon A, Zhu XG.** 2015. Meeting the global food demand of the future by engineering crop photosynthesis and yield potential. *Cell* **161**, 56–66.
- Losh JL, Young JN, Morel FM.** 2013. Rubisco is a small fraction of total protein in marine phytoplankton. *New Phytologist* **198**, 52–58.
- Mackinder LCM, Meyer MT, Mettler-altmann T, Chen V, Madeline C.** 2016. A repeat protein links Rubisco to form the eukaryotic carbon concentrating organelle. *Proceedings of the National Academy of Sciences, USA* **113**, 5958–5963.
- Mangan NM, Flamholz A, Hood RD, Milo R, Savage DF.** 2016. pH determines the energetic efficiency of the cyanobacterial CO₂ concentrating mechanism. *Proceedings of the National Academy of Sciences, USA* **113**, E5354–E5362.
- Manton I, Peterfi LS.** 1969. Observations on the fine structure of coccoliths, scales and the protoplast of a freshwater Coccolithophorid, *Hymenomonas roseola* Stein, with supplementary observations on the Protoplast of *Cricosphaera carterae*. *Proceedings of the Royal Society B: Biological Sciences* **172**, 1–15.
- McKay RM, Gibbs SP.** 1990. Phycoerythrin is absent from the pyrenoid of *Porphyridium cruentum*: photosynthetic implications. *Planta* **180**, 249–256.
- Morel FMM, Reinfelder JR, Roberts SB, Chamberlain CP, Lee JG, Yee D.** 1994. Zinc and carbon co-limitation of marine phytoplankton. *Nature* **369**, 740–742.
- Moritz M, Griffiths H.** 2013. Origins and diversity of eukaryotic CO₂-concentrating mechanisms: lessons for the future. *Journal of Experimental Botany* **64**, 769–786.
- Moroney JV, Ma Y, Frey WD, Fusilier KA, Pham TT, Simms TA, DiMario RJ, Yang J, Mukherjee B.** 2011. The carbonic anhydrase isoforms of *Chlamydomonas reinhardtii*: intracellular location, expression, and physiological roles. *Photosynthesis Research* **109**, 133–149.
- Nassoury N, Fritz L, Morse D.** 2001. Circadian changes in ribulose-1,5-bisphosphate carboxylase/oxygenase distribution inside individual chloroplasts can account for the rhythm in dinoflagellate carbon fixation. *The Plant Cell* **13**, 923–934.
- Okazaki M, Aruga S, Okamura Y.** 1992. Role of carbonic anhydrase in photosynthesis of unicellular marine algae coccolithophorids (Haptophyta). *Photosynthesis Research* **34**, 783–786.
- Raven JA, Cockell CS, De La Rocha CL.** 2008. The evolution of inorganic carbon concentrating mechanisms in photosynthesis. *Philosophical Transactions of the Royal Society B: Biological Sciences* **363**, 2641–2650.
- Raven JA, Giordano M, Beardall J, Maberly SC.** 2012. Algal evolution in relation to atmospheric CO₂: carboxylases, carbon-concentrating

mechanisms and carbon oxidation cycles. *Philosophical Transactions of the Royal Society B: Biological Sciences* **367**, 493–507.

Read BA, Kegel J, Klute MJ, et al. 2013. Pan genome of the phytoplankton *Emiliania* underpins its global distribution. *Nature* **499**, 209–213.

Reinfelder JR. 2011. Carbon concentrating mechanisms in eukaryotic marine phytoplankton. *Annual Review of Marine Science* **3**, 291–315.

Richlen M, Barber PH. 2005. A technique for the rapid extraction of microalgal DNA from single live and preserved cells. *Molecular Ecology Notes* **4**, 688–691.

Sage RF. 2002. Variation in the k_{cat} of Rubisco in C_3 and C_4 plants and some implications for photosynthetic performance at high and low temperature. *Journal of Experimental Botany* **53**, 609–620.

Sage RF, Khoshravesh R, Sage TL. 2014. From proto-Kranz to C_4 Kranz: building the bridge to C_4 photosynthesis. *Journal of Experimental Botany* **65**, 3341–3356.

Sage RF, Sage TL, Kocacinar F. 2012. Photorespiration and the evolution of C_4 photosynthesis. *Annual Review of Plant Biology* **63**, 19–47.

Savir Y, Noor E, Milo R, Tlustý T. 2010. Cross-species analysis traces adaptation of Rubisco toward optimality in a low-dimensional landscape. *Proceedings of the National Academy of Sciences, USA* **107**, 3475–3480.

Sharwood RE. 2017. Engineering chloroplasts to improve Rubisco catalysis: prospects for translating improvements into food and fiber crops. *New Phytologist* **213**, 494–510.

Sharwood RE, Ghannoum O, Kapralov MV, Gunn LH, Whitney SM. 2016a. Temperature responses of Rubisco from Paniceae grasses provide opportunities for improving C_3 photosynthesis. *Nature Plants* **2**, 16186.

Sharwood RE, Ghannoum O, Whitney SM. 2016b. Prospects for improving CO_2 fixation in C_3 -crops through understanding C_4 -Rubisco biogenesis and catalytic diversity. *Current Opinion in Plant Biology* **31**, 135–142.

Sharwood RE, Sonawane BV, Ghannoum O, Whitney SM. 2016c. Improved analysis of C_4 and C_3 photosynthesis via refined *in vitro* assays of their carbon fixation biochemistry. *Journal of Experimental Botany* **67**, 3137–3148.

Soto AR, Zheng H, Shoemaker D, Rodriguez J, Read BA, Wahlund TM. 2006. Identification and preliminary characterization of two cDNAs encoding unique carbonic anhydrases from the marine alga *Emiliania huxleyi*. *Applied and Environmental Microbiology* **72**, 5500–5511.

Tabita FR, Satagopan S, Hanson TE, Kreeel NE, Scott SS. 2008. Distinct form I, II, III, and IV Rubisco proteins from the three kingdoms of life provide clues about Rubisco evolution and structure/function relationships. *Journal of Experimental Botany* **59**, 1515–1524.

Tachibana M, Allen AE, Kikutani S, Endo Y, Bowler C, Matsuda Y. 2011. Localization of putative carbonic anhydrases in two marine diatoms, *Phaeodactylum tricornutum* and *Thalassiosira pseudonana*. *Photosynthesis Research* **109**, 205–221.

Tcherkez G. 2013. Modelling the reaction mechanism of ribulose-1,5-bisphosphate carboxylase/oxygenase and consequences for kinetic parameters. *Plant, Cell and Environment* **36**, 1586–1596.

Tcherkez G. 2016. The mechanism of Rubisco-catalysed oxygenation. *Plant, Cell and Environment* **39**, 983–997.

Tcherkez GGB, Farquhar GD, Andrews TJ. 2006. Despite slow catalysis and confused substrate specificity, all ribulose bisphosphate carboxylases may be nearly perfectly optimized. *Proceedings of the National Academy of Sciences, USA* **103**, 7246–7251.

Trimborn S, Langer G, Rost B. 2007. Effect of varying calcium concentrations and light intensities on calcification and photosynthesis in *Emiliania huxleyi*. *Limnology Oceanography* **52**, 2285–2293.

von Caemmerer S, Furbank RT. 2016. Strategies for improving C_4 photosynthesis. *Current Opinion in Plant Biology* **31**, 125–134.

Wang L, Yamano T, Takane S, et al. 2016. Chloroplast-mediated regulation of CO_2 -concentrating mechanism by Ca^{2+} -binding protein CAS in the green alga *Chlamydomonas reinhardtii*. *Proceedings of the National Academy of Sciences, USA* **113**, 12586–12591.

Wang Y, Stessman DJ, Spalding MH. 2015. The CO_2 concentrating mechanism and photosynthetic carbon assimilation in limiting CO_2 : how *Chlamydomonas* works against the gradient. *The Plant Journal* **82**, 429–448.

Whitney SM, Baldet P, Hudson GS, Andrews TJ. 2001. Form I Rubiscos from non-green algae are expressed abundantly but not assembled in tobacco chloroplasts. *The Plant Journal* **26**, 535–547.

Whitney SM, Houtz RL, Alonso H. 2011. Advancing our understanding and capacity to engineer nature's CO_2 -sequestering enzyme, Rubisco. *Plant Physiology* **155**, 27–35.

Yamano T, Sato E, Iguchi H, Fukuda Y, Fukuzawa H. 2015. Characterization of cooperative bicarbonate uptake into chloroplast stroma in the green alga *Chlamydomonas reinhardtii*. *Proceedings of the National Academy of Sciences, USA* **112**, 7315–7320.

Yoon HS, Hackett JD, Pinto G, Bhattacharya D. 2002. The single, ancient origin of chromist plastids. *Proceedings of the National Academy of Sciences, USA* **99**, 15507–15512.

Yoon S, Govind CK, Qiu H, Kim S-J, Dong J, Hinnebusch AG. 2004. Recruitment of the ArgR/Mcm1p repressor is stimulated by the activator Gcn4p: a self-checking activation mechanism. *Proceedings of the National Academy of Sciences, USA* **101**, 11713–11718.

Young JN, Heures AM, Sharwood RE, Rickaby RE, Morel FM, Whitney SM. 2016. Large variation in the Rubisco kinetics of diatoms reveals diversity among their carbon-concentrating mechanisms. *Journal of Experimental Botany* **67**, 3445–3456.

Young JN, Rickaby RE, Kapralov MV, Filatov DA. 2012. Adaptive signals in algal Rubisco reveal a history of ancient atmospheric carbon dioxide. *Philosophical Transactions of the Royal Society B: Biological Sciences* **367**, 483–492.